Molecular-Level Characterization of Changes in the Mechanical Properties of Wood in Response to Thermal Treatment

Dong Wang
Northwestern Polytechnical University https://orcid.org/0000-0002-4235-8719
Feng Fu
Chinese Academy of Forestry Research Institute of Wood Industry
Lanying Lin (linly@caf.ac.cn)
Chinese Academy of Forestry Research Institute of Wood Industry

Research Article

Keywords: Thermal treatment, FTIR spectroscopy, Hemicellulose, Cellulose microfibrils, Mechanical properties

Posted Date: September 20th, 2021

DOI: https://doi.org/10.21203/rs.3.rs-882939/v1

Version of Record: A version of this preprint was published at Cellulose on March 8th, 2022. See the published version at https://doi.org/10.1007/s10570-022-04471-3.

Abstract

Thermal treatment can improve the dimensional stability of wood, but it also decreases wood's stiffness and increases its brittleness. In this paper, combining FTIR spectroscopy and mechanical analysis was used to *in-situ* study the molecular-level responses to stresses and analyze mechanical interactions among components in thermally-treated wood. For both untreated and treated woods, the cellulose was the longitudinal tensile load-bearing component of wood, but the lignin participated in the load transfer in the fiber direction. Moreover, the FTIR results indicated that hemicellulose degradation, as the interface between cellulose and lignin, decreased shear slipping between microfibrils. The interfacial material degradation also caused the wood's stiffness and mechanical responses of the matrix along the cell transverse direction decrease. Upon increasing the heat treatment intensity, the cellulose microfibrils rearranged along the cell axis, resulting in the ability of the cell wall to resist deformation and the wood's stiffness being increased.

1. Introduction

Due to increased focus on energy conservation and pollution reduction, wooden materials are widely used in various fields because wood is a renewable resource with an exceptional strength-to-weight ratio; however, the utilization of wooden materials during outdoor service is restricted by their lack of dimensional stability, low resistance to decay, and poor durability (Guo et al., 2015; Mastouri et al., 2021). Many wood modification technologies have rapidly advanced, including chemical, thermal, and other treatment processes (Hill 2006).

Thermal modification between 160 ℃ and 240 ℃ has been used to improve the dimensional stability and microbial resistance of wood (Sandberg et al., 2013; Hill et al., 2021), but several undesirable changes also occur which, depending upon the treatment intensity, can cause losses in both strength and stiffness (Bekhta and Niemz 2003; Windeisen et al., 2009; Rautkari and Hill 2014; Candelier et al., 2016). Changes in the chemical structure of wood are also aggravated due to thermal treatment, which can increase its brittleness and decrease its toughness (Hughes et al., 2015). Thus, thermal treatment changes the natural advantages of wood, i.e., its high strength and toughness (Barthelat et al., 2016; Berglund et al., 2020). A key point in the wood thermal modification field is how to characterize changes in the mechanical properties of thermally-treated wood at the molecular level.

Previous studies have clearly shown that thermal treatment causes massive chemical structure changes in wood polymers. The hemicelluloses and amorphous regions of cellulose are more susceptible to thermal degradation, which increases wood's crystallinity and dimensional stability (Hill et al., 2021; Alén et al., 2002; Lin et al., 2018; Yin et al., 2017). In addition, cellulose crystallite dimensions significantly increased after thermal treatment due to the rearrangement of adjacent cellulose chains (Inagaki et al., 2010; Guo et al., 2016). ^{13}C CPMAS NMR spectroscopy was used to show that in softwood lignin, the methoxyl group content decreased, leading to a more condensed lignin structure (Wikberg and Maunu 2004). The increased wood polymer interaction due to the heat treatment was most likely caused by

cross-linkages being formed between the different components of the cellulose, lignin and xylan moieties (Salmén et al., 2008); however, there is no direct evidence for determining how these chemical structural changes affect the mechanical properties of thermally-treated wood.

Combining FTIR spectroscopy and mechanical analysis is important method for obtaining information on the internal structure of wood polymers, such as ploymer orientation (Salmén and Bergstrm 2009), interaction between wood ploymers (Åkerholm and Salmén 2001; Hofstetter et al., 2006). Furthermore, the technology also provides an *in situ* method to study molecular-level responses to stresses and analyze mechanical interactions among components in wood-based materials (Hinterstoisser et al., 2003; Salmén et al., 2016; Peng et al., 2019; Stevanic and Salmén 2020). In this paper, to elucidate the influence of the thermal treatment on the chemical structure and mechanical properties of wood, thermal treatment was conducted at different temperatures. Static tension and dynamic FTIR spectra were used to investigate the effects of chemical structure changes on the mechanical properties of thermally-treated wood at the molecular scale.

2. Materials And Methods

2.1 Materials

Spruce wood (*Picea asperata*, about 31 growth rings) was obtained from Shanghai province, China. Wood specimens with dimensions of 35 cm × 2 cm × 20 cm in the longitudinal (*L*), radial (*R*), and tangential (*T*) directions were prepared. All specimens were oven-dried at 65 °C for 48 h and then at 103 °C for 24 h, and were then divided into six groups. Their average density was 0.41 g/cm^3.

2.2 Methods

2.2.1 Thermal treatment processing

Thermal treatments were conducted in a vacuum vessel equipped with two metal heating plates. First, the specimens were clamped between two metal heating plates, then residual gas was removed from the vessel by pulling a vacuum of -0.9 MPa for 1 h. Then, the two metal heating plates were heated to a predetermined temperature and held for 1 h. The temperature of the metal plates was set to 160 ℃, 180 ℃, 200 ℃, and 220 ℃, respectively. Finally, the vacuum was unloaded, and the specimens were taken out.

2.2.2 Chemical composition analysis

Chemical composition analysis was performed according to a previous research method (Wang et al., 2014). The untreated and treated samples were mashed to a length of 0.18–0.25 cm. Holocellulose analysis was performed according to Wises's sodium chlorite method, cellulose was determined by Kürschner-Hoffner's nitric acid method, and the lignin content was determined by acid-insoluble Klason

lignin. The hemicelluloses content was determined by subtracting the cellulose content from the holocellulose content. All percentages of chemical constituents were averages of three replicates.

2.2.3 X-ray diffraction measurements

The untreated and treated samples were ground using an ordinary mill (Speed was 32000 revolutions per minute) and sieved using a steel sieves (60 mesh). The samples of 0.5 mm in thickness and 7 mm in diameter were formed from 0.05 g of the sieved powder by pressing in a mold under 10kN. Three samples were formed for each treatment condition. The XRD patterns of the samples were measured using an X-ray diffractometer reflection mode (D8 Advance, BRUKER, Germany), with Ni-filtered CuKα radiation (λ= 0.154 nm) at 40 kV and 40 mA. The reflection intensity was recorded through the scanning angle (2θ) range of 5–45° at a scanning speed of 1°/min, as shown in FigS.1 (Supplementary materials Figure 1). Peaks in diffraction intensity cure were resolved using PeakFitR (Sea-Solve Software, Inc., Richmond, CA). The crystallinity index (*CI*) was calculated by the Segal method (Segal et al. 1959) and the following equation:

$$CI = \frac{I_{200} - I_{am}}{I_{200}} \times 100\% \quad (1)$$

where I_{200} is the maximum reflection intensity of the cellulose (200) peak, and I_{am} is the minimum reflection intensity near the 2θ angle of 18.5°.

The crystal width is defined as the average thickness of cellulose crystallites perpendicular to the cellulose (200) plane (D_{200}). Based on the Scherrer equation (Alexander 1969), D_{200} was calculated by the following equation:

$$D_{200} = \frac{K\lambda}{\beta_{1/2} \cos\theta_{200}} \times 100\% \quad (2)$$

where K is the Scherrer constant (K = 0.9), λ is the wavelength of the X-rays (0.1542 nm), and $\beta_{1/2}$ is the half bandwidth (full width at half maximum, FWHM) of the (200) peak in radians, and θ_{200} is the Bragg angle for the (200) plane.

The microfibril angles (MFA) of thermally-treated wood samples were measured using an X-ray diffractometer transmission mode (D8 Advance, BRUKER, Germany). The samples with dimensions of 20 mm × 10 mm × 1 mm in the L, T, and R directions were fixed with double-side tape in a platform holder, with the direction of the zero scale of the platform holder parallel to the sample fiber axis. The platform rotated 360° at a rate of 0.5°/step. In the test, the incident light was perpendicular to the sample chord plane, exhibiting an angle 2θ with the receiving light. Of particular note, the relationship between (200) reflections and the azimuth angle could be measured when the setting diffraction angle 2θ was 22.1°. Subsequently, diffraction curves were fitted by GaussAmp bimodal functions (Hu et al. 2017) and the T-

method average MFA values was calculated by utilizing the well-established 0.6 T method (Cave 1966), as shown in FigS.2 (Supplementary materials Figure 2).

2.2.4 Static-loading FTIR and Dynamic FTIR spectroscopies

Static tension and dynamic Fourier-transform infrared (FTIR) spectra were recorded on a VERTEX 70 spectrometer combined with a polymer stretcher kit (A555/Z, Bruker, Ettlingen, Germany). The samples used in the static tension and dynamic FTIR experiments were cut into dimensions of 25 mm (*L*) × 15 mm (*T*) × 20 μm (*R*), with the direction of the fiber axis parallel to the load direction. Before testing, samples were equilibrated in the sample chamber for 2 h (25 ºC, RH 65%).

Static tension FTIR spectra were recorded at different tensile strains to study the molecular responses to the loading of thermally-treated wood (Salmén and Bergstrm, 2009). A sample was mounted in the stretcher kit, with the longitudinal direction of specimens parallel to the tensile direction. The spectra were recorded at a 1 cm^{-1} resolution, using an average of 16 scans at each strain. Five samples were tested at each treatment intensity. The spectra were baseline corrected at 1800 cm^{-1} and 2300 cm^{-1}, and the 1^{st} derivative of each spectrum was used to determine the peak position for each specific absorption peak of wood polymers (Wang et al., 2020).

Dynamic FTIR spectroscopy can be used to observe the molecular responses of wood constituents in strained wood (Salmén et al., 2016; Wang et al., 2020). The samples were pre-stretched in the longitudinal direction by using the stretcher to apply a load of 4 N (approximately 50% of the breaking stress). A small sinusoidal strain (< 0.3% by a 4 N pre-stretched load) with a frequency of 16 Hz was applied to the sample, and the transition dipole responses were monitored as a phase lag with respect to the external perturbation. An interferometer was run in a step-scan mode with a scanning speed of 1.0 Hz. An in-phase spectrum was obtained to indicate immediate changes or elastic responses (0° phase loss angle) and an out-of-phase spectrum was used to represent the time-delayed changes or viscous response (90° phase loss angle). IR radiation was polarized by a wire grid polarizer at 0° relative to the stretching direction. An optical filter was added after the polarizer to reduce the spectral range 3000–700 cm^{-1}. Three samples of each thermal treatment intensity were tested. The spectra were baseline corrected. All spectra were baseline corrected at 2300 cm^{-1}, 1800 cm^{-1}, and 700 cm^{-1}, and were normalized to 1 at 1435 cm^{-1} (Salmén et al., 2008).

3. Results And Discussion

3.1 Chemical compositions

As shown in Fig. 1, the bar chart and line graphs show changes in the relative percentages of the wood chemical composition. The least thermally-stable hemicelluloses began to degrade at 160 ℃, consistent with a previous study (Alén et al., 2002), and the degradation rates of hemicelluloses at 160 ℃ and 220 ℃ were faster compared with those at 180 ℃ and 200 ℃. Cellulose has better thermal stability than

hemicelluloses (Inagaki et al., 2010; Guo et al., 2016). The relative percentage of cellulose changed very little from 160 ℃ to 200 ℃, but it began to degrade at 220 ℃, but its relative percentage only decreased by 1.5%. Finally, the loss of polysaccharides during heating also increased the relative lignin content.

3.2 Cellulose crystalline structure

Table 1 displays the crystallinity *CI* and crystal width of thermally-treated wood as functions of temperature. The crystallinity and crystal width of thermally-treated wood samples increased with respect to the untreated samples. For the untreated wood samples, the *CI* was 48.32%, in agreement with a previous study (Andersson et al., 2005). The *CI* of the wood samples thermally-treated from 160 ℃ to 200 ℃ increased to 53.96%, which is similar to variations in the *CI* after heating in air or nitrogen (Kubojima et al., 1998); however, there was a slight decrease in the crystallinity at 220 ℃. The average crystallite thickness (D_{200}) of the untreated wood was 2.77 nm, and the values of the thermally-treated wood from 160 ℃ to 220 ℃ increased to 2.97 nm, indicating a 7.2% increase compared with the untreated sample.

Table 1
XRD and static tensile FTIR analysis results of different thermally-treated samples

Treatment Temp.	*CI* (%)	D_{200} (nm)	MFA (°)	Bandshift of cellulose C-O-C ($cm^{-1}/d\varepsilon$)
Untreated	48.32 ± 0.32^{D}	2.77 ± 0.02^{D}	19.81 ± 0.41^{A}	$y = -2.92 \times \varepsilon - 0.50^{C}$ $R^2 = 0.87$
160 ℃	49.48 ± 0.06^{C}	2.83 ± 0.01^{C}	19.71 ± 0.31^{A}	$y = -3.15 \times \varepsilon - 0.06^{B}$ $R^2 = 0.74$
180 ℃	52.54 ± 0.19^{B}	2.90 ± 0.02^{B}	19.48 ± 0.62^{A}	$y = -3.31 \times \varepsilon - 0.06^{A}$ $R^2 = 0.87$
200 ℃	53.96 ± 0.63^{A}	2.95 ± 0.04^{A}	19.41 ± 0.38^{A}	$y = -3.36 \times \varepsilon + 0.01^{A}$ $R^2 = 0.87$
220 ℃	53.27 ± 0.83^{AB}	2.97 ± 0.02^{A}	18.56 ± 0.24^{B}	$y = -2.70 \times \varepsilon - 0.10^{D}$ $R^2 = 0.81$

Note: Superscripts A, B, C, D, denoted analysis of variance, same letter indicated no statistically significant difference at a significance level of 5 %.

One-factor ANOVA was used to investigate the statistical significance of the crystallinity and cellulose crystallite dimensions as a function of temperature (Table 1). Analysis showed that temperature (160–

200 ℃) had a significant influence on the crystallinity and cellulose crystallite dimensions at a significance level of 5%. The main reason for the increase in the degree of crystallinity was hemicellulose degradation, which also was related to the rearrangement of amorphous cellulose molecules (Hori and Wada 2005; Xing et al., 2016; Yin et al., 2017); however, the crystallinity and cellulose crystallite dimensions of the sample treated at 220 ℃ were not significantly different than those of the sample treated at 200 ℃. The reason could be that cellulose began to degrade at 220 ℃, and it only decreased by 1.5% (Fig. 1). This is supported by previous results that investigated crystalline cellulose degradation in the temperature range 300–340 ℃ (Kim et al., 2001; Kačíkováa et al., 2013).

3.3 Arrangement of cellulose microfibril

As shown in Table 1, the average MFA of the untreated sample wood was 19.81°. The MFAs of all thermally-treated samples only slightly changed compared with the untreated sample. The mean MFAs decreased from 19.71° to 18.56° upon increasing the temperature from 160 ℃ to 220 ℃, and the standard deviations were in the range 0.31–0.62°. The one-factor ANOVA results indicated no systematic variation in the MFA distributions with temperature from 160 ℃ to 200 ℃ (Table 1), but for the sample treated at 220 ℃, the MFA significantly decreased to 18.56° compared with the untreated and other thermally-treated samples. The most probable reason was that the degradation of polyoses near cellulose microfibrils and lignin softening during thermal treatment caused partial reorientation of the cellulose microfibrils (Zollfrank and Fromm 2009; Björn, 2010).

3.4 Results of static tension FTIR

Figure 2 shows the spectral changes as a function of longitudinal tensile strain applied to the thermally-treated (180 ℃) and untreated wood samples. The absorption peak at 1160 cm^{-1} (glycosidic C-O-C vibration of cellulose) underwent a substantial shift to lower wave numbers as the tensile strain increases, which signified an increase in the length of the covalent bonds involved in the vibration absorption, i.e., a decrease in the force constant of the bond (Wool 1981). This response was attributed to the deformation of the glycosidic bond of cellulose, which has also been observed in previous studies of normal wood (Eichhorn et al., 2001; Salmén and Bergström 2009; Wang et al., 2020). Furthermore, as shown in Fig. 2, the longitudinal tensile strain of 180 ℃ treated sample was less than that of the untreated sample, but the bandshifts of the cellulose glycosidic bond before the sample break were more.

To examine the effect of the treatment temperature on the deformation of cellulose, the shift in the absorption peak at 1160 cm^{-1} was plotted against the applied strain. The peak shifted approximately linearly with the tensile strain towards a lower wavenumber ($R^2 > 0.7$, Fig. 3). As shown in Table 1, the shift ratio of the untreated sample was − 2.92 $cm^{-1}/d\varepsilon$, and the shift ratios of the samples treated from 160–200 ℃ increased upon increasing the temperature; however, the shift ratio of the sample treated at 220 ℃ was − 2.72 $cm^{-1}/d\varepsilon$, which was smaller than that of the other samples. The ANOVA results indicated that temperatures from 160 ℃ to 180 ℃ significantly influenced the shift of the absorption peak at a significance level of 5%, but there was no significant difference between the samples treated at

180 ℃ and 200 ℃. Finally, the shift ratio of the sample treated at 220 ℃ was significantly reduced compared with the untreated and other treated samples.

For hemicelluloses and lignin, the characteristic peaks at 1735 cm^{-1}, 1510 cm^{-1}, and 810 cm^{-1}, belonged to C = O stretching vibrations in the O = C-OH group of the glucuronic acid unit in xylan (Åkerholm and Salmén, 2001), to the aromatic skeletal vibrations and C = O stretching of lignin (Faix, 1991), and to vibrations caused by equatorial hydrogens on the C_2 atom in the mannose residues of glucomannan (Åkerholm and Salmén, 2001; Guo, et al. 2015). As shown in Fig. 2, for the untreated or treated wood samples, no substantial shift in the specific absorption peaks of hemicellulose and lignin occurred, which has also been widely confirmed by earlier researches on normal wood (Eichhorn, et al., 2001; Salmén and Bergstrm, 2009; Wang, et al., 2020). Taking the characteristic peak at 1510 cm^{-1} of lignin as an example, the shift in the characteristic peak of the matrix was almost zero at all tensile strains (Fig. 3).

A schematic showing the cell wall deformation of wood is shown in Fig. 4. The S_2 layer of the wood cell wall, generally the thickest with the smallest distribution of MFA, is the layer directly responsible for the axial mechanics of cells (Jarvis, 2009). When the tracheid was stretched to a strain (ε_0) along the cell axial direction, the strain along the microfibril longitudinal direction was $\varepsilon_0/\cos\theta$, which was the sum of shear slipping strain between microfibrils (ε_2) and the stretching strain of microfibril itself (ε_1) (Adler and Buehler, 2013), as shown in Eq. (3):

$$\frac{\varepsilon_0}{\cos\theta} = \varepsilon_1 + \varepsilon_2 \qquad (3)$$

It was assumed that the MFA (θ) did not change during stretching, and then the first derivative with respect to the deformation (ε_0) was calculated using Eq. (4):

$$\frac{1}{\cos\theta} = \frac{d\varepsilon_1}{d\varepsilon_0} + \frac{d\varepsilon_2}{d\varepsilon_0} \qquad (4)$$

The former deformation was a relationship of the deformation of cellulose, which was related to the shift in the absorption peak at 1160 cm^{-1}. The later deformation had contributions from shear slipping between microfibrils, which was related to bridges between microfibrils, such as hemicelluloses and intermolecular hydrogen bonds (Kretschmann 2003).

For the samples treated at 160–200 ℃, the absolute values of the shift ratios of the cellulose characteristic peak increased upon increasing the temperature, which indicated the stretching deformation of cellulose increased with the thermal treatment temperature. According to Eq. (4) ($1/\cos\theta$ = Constant), increasing the stretching deformation of cellulose decreased shear slipping between cellulose microfibrils. This might lead to the toughness of the treated wood decreasing, or the brittleness increasing. Hemicelluloses, as the interface between cellulose and lignin, caused the microfibrils to

undergo shear slip and provided ‘Velcro mechanics’ in wood, which increased the plastic deformation and toughness of cell walls (Kretschmann 2003; Adler and Buehler, 2013). For the samples treated at 220 ℃, a decrease in the MFA was obvious (Table 1), which decreased the value of $1/\cos\theta$. This indicated that the stretching deformation of cellulose and the shift ratio of the C-O-C bonds of cellulose decreased; therefore, shear slipping deformation between microfibrils and stretching deformation of wood microfibrils decreased. The MFA rearrangement along cell axis also might lead to a decrease in the toughness of thermally-treated wood.

3.5 Results of dynamic FTIR

Figure 5 shows the mean dynamic FTIR spectra of untreated wood samples with an IR beam polarized 0° and 90° relative to the strain direction. The in-phase spectrum is a measure of the elastic-like response, and the out-of-phase spectrum is associated with the viscous-like behavior (Hofstetter et al., 2006; Åkerholm and Salmén 2003). In the 0° and 90° polarization modes, the signal intensities of the in-phase spectra in both polarization directions were several times higher than those of the out-of-phase spectra, which mean that there were no molecular groups with a time-delayed response (Åkerholm and Salmén 2003).

Two clear split bands at 1169–1149 cm^{-1} and 1435–1420 cm^{-1} can be seen in the in-phase spectrum at 0° polarization. These signals appeared because cellulose microfibrils are the load-bearing components of wood. The C-O-H bending vibrations of the CH_2-OH group appeared at 1435 cm^{-1}, and the cellulose skeleton vibrations, including the C-O-C bridge stretching, appeared at 1169 cm^{-1} (Hinterstoisser et al., 2001). A schematic of the cell wall structure indicating the main structure and alignment of cellulose, hemicellulose, and lignin is shown in Fig. 6. The microfibril arrangement in the S_2 layer was parallel to the cell axis; therefore, the two split peaks at 0° polarization reflected changes in the energy of these bonds of cellulose due to stretching and deformation by the applied load (Hinterstoisser et al., 2003).

At 90° polarization, the two split peaks of cellulose disappeared in the in-phase spectrum in Fig. 5, but two single peaks of lignin at 90° polarization can be seen. At 1035 cm^{-1}, a peak appeared due to C-O deformation and aromatic C-H deformation in lignin, and the peak at 1510 cm^{-1} was assigned to the aromatic structure of lignin (Faix 1991). In addition, a weaker peak at 1730 cm^{-1} due to xylan can also be seen in Fig. 5 (Collier, et al., 1992). As shown in Fig. 6, in softwood, xylan and lignin are closely associated, and gulcomannan crosslinks on the surface of microfibrils (Åkerholm and Salmén 2001). When the wood sample was stretched, a contraction perpendicular to the strain direction occurred due to the Poisson effect of the material (Bergander and Salmén 2002).

Figure 7 presents the mean spectra of the thermally-treated wood samples at 0° polarization. There are two split peaks at 1169 cm^{-1} and 1435 cm^{-1} related to cellulose, but their intensities in the spectra of thermally-treated samples were different. For the samples treated from 160 ℃ to 200 ℃, the intensities of the two split peaks decreased upon increasing the temperature, which indicated that the elastic-like response of cellulose and the stiffness of thermally-treated wood were decreased (Hofstetter et al., 2006;

Åkerholm and Salmén 2003). The main reason for this was that the hemicelluloses, as the microfibril-matrix interface, crosslinked on the surface of the microfibrils, which increased the stiffness of the cell wall (Berglund 2020). This was also demonstrated by the relationship between the hemicellulose content and elastic modulus of thermally-treated wood (Kačíková et al., 2013), but for the sample treated at 220 °C, the intensities of the two split peaks increased, which indicated that the stiffness of the sample increased because the MFA decreased (Table 1).

The mean dynamic spectra of thermally-treated samples at 90° polarization are shown in Fig. 8. The intensities of many peaks decreased upon increasing the treatment temperature. For example, the characteristic peak of xylan at 1730 cm^{-1} disappeared in the spectra of thermally-treated samples. In the in-phase spectra, the peaks at 1510 cm^{-1} and 1200–1300 cm^{-1}, which were related to the C-C and Caryl-O vibrations of lignin (Collier et al., 1992; Salmén et al., 2008), remained, but their peak intensities decreased upon increasing the treatment temperature. Finally, the peak at 1035 cm^{-1}, assigned to the aromatic C-H deformation of lignin, also decreased upon increasing the treatment temperature. The main reason for this was hemicellulose degradation, particularly xylan, which led to the disappearance of the characteristic peak of xylan at 1730 cm^{-1}. The degradation of xylan, as the cellulose-lignin bridge material in softwood, may have also resulted in a decrease in the mechanical responses of lignin in the cell transverse direction. Finally, the decrease in the intensities of several peaks in the lignin spectra might indicate that cellulose and lignin did not cross-linking occur.

4. Conclusion

Thermal treatment greatly changed the chemical structure of wood, including changes in the interactions between wood components, degradation, crystallinity increase, and microfibril orientation rearrangement. The FTIR spectra indicated that wood's chemical structure changed after thermal treatment, which resulted in large changes in its mechanical properties. The degradation of hemicellulose, as the interface between cellulose and lignin, resulted in shear slipping between microfibrils. In addition, the interface material degradation decreased the wood stiffness along the cell axis, as well as the mechanical response of the matrix along the cell transverse direction. Upon increasing the heat treatment temperature, the microfibrils rearranged along the cell axis, which indicated that the ability of the cell wall to resist deformation increased, and the wood stiffness recovered. These structures and mechanical property changes increased the brittleness of thermally-treated wood.

Declarations

CRediT authorship contribution statement

Dong Wang: Conceptualization, Methodology, Investigation, Formal analysis, Writing – original draft, Visualization. **Lanying Lin**: Conceptualization, Writing – review and editing. **Feng Fu**: Conceptualization, Writing – review and editing.

Acknowledgment

The authors gratefully acknowledge the financial support of the Nature Science Foundation of China (No.32101458) and the Fundamental Research Funds for the Central Universities (D5000210672).

Declaration of competing interest

The authors declare that they have no known competing financial interests or personal relationships that could have appeared to influence the work reported in this paper.

References

1. Adler DC, Buehler MJ (2013) Mesoscale mechanics of wood cell walls under axial strain. Soft Matter 9: 7138-7144. https://doi.org/ 10.1039/c3sm50183c
2. Åkerholm M, Salmén L (2001) Interactions between wood polymers studied by dynamic FTIR spectroscopy. Polymer 42: 963-969. https://doi.org/10.1016/S0032-3861(00)00434-1
3. Alén R, Kotilainen R, Zaman A (2002) Thermochemical behavior of Norway spruce (*Picea abies*) at 180–225 °C. Wood Sci Technol 36: 163–171. https://doi.org/10.1007/s00226-001-0133-1
4. Alexander LE (1969) X-ray diffraction methods in polymer science. Wiley, Amsterdam, pp 423–424.
5. Andersson S, Serimaa R, Vaeaenaenen T, Paakkari T, Jaemsae S, Viitaniemi P (2005) X-ray scattering studies of thermally modified scots pine (*Pinus sylvestris* L.). Holzforschung 35: 155-427. https://doi.org/10.1515/HF.2005.069
6. Barthelat F, Yin Z, Buehler M (2016) Structure and mechanics of interfaces in biological materials. Nat Rev Mater 16007 https://doi.org/10.1038/natrevmats.2016.7
7. Berglund J, Mikkelsen D, Flanagan BM, Dhital S, Vilaplana F (2020) Wood hemicelluloses exert distinct biomechanical contributions to cellulose fibrillar networks. Nat Commun 11: 4692. https://doi.org/10.1038/s41467-020-18390-z
8. Bergander A, Salmén L (2002) Cell wall properties and their effects on the mechanical properties of fibers. J Mater Sci 37: 151-156. https://doi.org/10.1023/A:1013115925679
9. Bekhta P, Niemz P (2003) Effect of high temperature on the change in color, dimensional stability and mechanical properties of spruce wood. Holzforschung 57: 539-546. https://doi.org/10.1515/HF.2003.080
10. Björn B, Cordt Z, Oliver F, Jörg F, Mathias G, Karsten D (2010) Micromechanics and ultrastructure of pyrolysed softwood cell walls. Acta Biomater 6: 4345-4351. https://doi.org/10.1016/j.actbio.2010.05.026
11. Candelier K, Thevenon MF, Petrissans A, Dumarcay S, Gerardin P, Petrissans M (2016) Control of wood thermal treatment and its effects on decay resistance: a review. Ann Forest Sci 73: 571-583. https://doi.org/10.1007/s13595-016-0541-x
12. Cave I (1966) Theory of X-ray measurement of microfibril angle in wood. For Prod J 16:37–43.

13. Collier WE, Schultz TP, Kalasinsky VF (1992) Infrared study of lignin: reexamination of aryl-alkyl ether C-O stretching peak assignments. Holzforschung 46: 523-528. https://doi.org/10.1515/hfsg.1992.46.6.523
14. Eichhorn SJ, Sirichaisit J, Young RJ (2001) Deformation mechanisms in cellulose fibres, paper and wood. J Mater Sci 36: 3129-3135. https://doi.org/10.1023/A:1017969916020
15. Faix O (1991) Classification of lignin from different botanical origins by FT-IR spectroscopy. Holzforschung 45: 21-27. https://doi.org/10.1515/hfsg.1991.45.s1.21
16. Guo J, Yin YF, Song KL, Yin YF (2015) Changes of wood cell walls in response to hygro-mechanical steam treatment. Carbohyd Polym 115: 207–214. https://doi.org/10.1016/j.carbpol.2014.08.040
17. Guo J, Rennhofer H, Yin Y, Lichtenegger, HC (2016) The influence of thermo-hygro-mechanical treatment on the micro- and nanoscale architecture of wood cell walls using small- and wide-angle x-ray scattering. Cellulose 23: 2325-2340. https://doi.org/10.1007/s10570-016-0982-2
18. Hill CAS (2006) Wood modification: Chemical, thermal and other processes. NewYork, NY: Wiley Press.
19. Hill C, Altgen M, Rautkari L (2021) Thermal modification of wood—a review: chemical changes and hygroscopicity. J Mater Sci 56: 6581-6614. https://doi.org/10.1007/s10853-020-05722-z
20. Hinterstoisser B, Åkerholm M, Salmén L (2003) Load distribution in native cellulose. Biomacromolecules 4: 1232-1237. https://doi.org/10.1021/bm030017k
21. Hori R, Wada M (2005) The thermal expansion of wood cellulose crystals. Cellulose 12:479. https://doi.org/10.1007/s10570-005-5967-5
22. Hinterstoisser B, Åkerholm M, Salmén L (2001) Effect of fiber orientation in dynamic FTIR study on native cellulose. Carbohyd Res 334: 27-37. https://doi.org/10.1016/S0008-6215(01)00167-7
23. Hofstetter K, Hinterstoisser B, Salmén L (2006) Moisture uptake in native cellulose - the roles of different hydrogen bonds: a dynamic FT-IR study using deuterium exchange. Cellulose 13: 131-145. https://doi.org/10.1007/s10570-006-9055-2
24. Hughes M, Hill C, Pfriem A (2015) The toughness of hygrothermally modified wood. Holzforschung 69: 851-862. https://doi.org/10.1515/hf-2014-0184
25. Hu K, Huang Y, Fei B, Yao C, Zhao C (2017) Investigation of the multilayered structure and microfibril angle of different types of bamboo cell walls at the micro/nano level using a LC-PolScope imaging system. Cellulose 24: 4611–4625. https://doi.org/10.1007/s10570-017-1447-y
26. Inagaki T, Siesler HW, Mitsui K, Tsuchikawa S (2010) Difference of the crystal structure of cellulose in wood after hydrothermal and aging degradation: a NIR spectroscopy and XRD study. Biomacromolecules 11: 2300-2305. https://doi.org/10.1021/bm100403y
27. Jarvis MC (2009) Plant cell walls: supramolecular assembly, signalling and stress. Struct Chem 20: 245–253. https://doi.org/10.1007/s11224-009-9427-y
28. Kačíková D, Kačík F, Čabalová I, Ďurkovič J (2013) Effects of thermal treatment on chemical, mechanical and colour traits in Norway spruce wood. Bioresource Technol 144: 669–674.

https://doi.org/10.1016/j.biortech.2013.06.110

29. Kretschmann D (2003) Nature materials: Velcro mechanics in wood. Nat Mater 2: 775. https://doi.org/10.1038/nmat1025
30. Kim DY, Nishiyama Y, Wada M, Kuga S, Okano T (2001) Thermal decomposition of cellulose crystallites in wood. Holzforschung 55: 521-524. https://doi.org/10.1515/HF.2001.084
31. Kubojima Y, Okano T, Ohta M (1998) Vibrational properties of Sitka spruce heat-treated in nitrogen gas. J Wood Sci 44: 73–77. https://doi.org/10.1007/BF00521878
32. Lin BJ, Colin B, Chen WH, Petrissans A, Rousset P, Petrissans M (2018) Thermal degradation and compositional changes of wood treated in a semi-industrial scale reactor in vacuum. J Ana App Pyrol 130: 8-18. https://doi.org/10.1016/j.jaap.2018.02.005
33. Mastouri A, Efhamisisi D, Shirmohammadli Y, Oladi R (2021) Physicochemical properties of thermally treated poplar wood in silicone and rapeseed oils: A comparative study. J Build Eng 43:102511. https://doi.org/10.1016/j.jobe.2021.102511
34. Peng H, Salmén L, Jiang J, Lu J (2019) Contribution of lignin to the stress transfer in compression wood viewed by tensile FTIR loading. Holzforschung 74: 459-467. https://doi.org/10.1515/hf-2019-0206
35. Rautkari L, Hill C (2014) Effect of initial moisture content on the anti-swelling efficiency of thermally modified scots pine sapwood treated in a high-pressure reactor under saturated steam. Holzforschung 68: 323-326. https://doi.org/10.1515/hf-2013-0078
36. Salmén L, Bergström E (2009) Cellulose structural arrangement in relation to spectral changes in tensile loading FTIR. Cellulose 16: 975–982. https://doi.org/10.1007/s10570-009-9331-z
37. Salmén L, Stevanic JS, Olsson AM (2016) Contribution of lignin to the strength properties in wood fibres studied by dynamic FTIR spectroscopy and dynamic mechanical analysis (DMA). Holzforschung 70: 1155-1163. https://doi.org/10.1515/hf-2016-0050
38. Salmén L, Possler H, Stevanic JS, Stanzl-Tschegg SE (2008) Analysis of thermally treated wood samples using dynamic FT-IR-spectroscopy. Holzforschung 62: 676-678. https://doi.org/10.1515/HF.2008.113
39. Sandberg D, Haller P, Navi P (2013) Thermo-hydro and thermo-hydro-mechanical wood processing: an opportunity for future environmentally friendly wood products. Wood Mater Sci Eng 8: 64-88. https://doi.org/10.1080/17480272.2012.751935
40. Segal L, Creely JJ, Martin AE, Conrad CM (1959) An empirical method for estimating the degree of crystallinity of native cellulose using the X-ray diffractometer. Text Res J 29:786–794. https://doi.org/10.1177/004051755902901003
41. Stevanic JS, Salmén L (2020) Molecular origin of mechano-sorptive creep in cellulosic fibres. Carbohyd Polym 230: 115615. https://doi.org/10.1016/j.carbpol.2019.115615
42. Windeisen E, Bächle H, Zimmer B, Wegener G (2009) Relations between chemical changes and mechanical properties of thermally treated wood 10th EWLP, Stockholm, Sweden, August 25 – 28, 2008. Holzforschung 63: 773 – 778. https://doi.org/10.1515/HF.2009.084

43. Wikberg H, Maunu SL (2004) Characterisation of thermally modified hard- and softwoods by ^{13}C CPMAS NMR. Carbohyd Polym 58: 461-466. https://doi.org/10.1016/j.carbpol.2004.08.008
44. Wang X, Deng Y, Wang S, Min C, Meng Y, Pham T (2014) Evaluation of the effects of compression combined with heat treatment by nanoindentation (NI) of poplar cell walls. Holzforschung, 68: 167-173. https://doi.org/10.1515/hf-2013-0084
45. Wool RP (2010) Measurements of infrared frequency shifts in stressed polymers. J Polym Sci Pol Chem 19: 449 – 457. https://doi.org/10.1002/pol.1981.180190305
46. Wang D, Lin L, Fu F (2020) Deformation mechanisms of wood cell walls under tensile loading: a comparative study of compression wood (CW) and normal wood (NW). Cellulose 27: 4161–4172. https://doi.org/10.1007/s10570-020-03095-9
47. Xing D, Li J, Wang X, Wang S (2016) In situ measurement of heat-treated wood cell wall at elevated temperature by nanoindentation. Ind Crop Prod 87: 142-149. https://doi.org/10.1016/j.indcrop.2016.04.017
48. Yin J, Yuan T, Yun L, Song K, Yin Y (2017) Effect of compression combined with steam treatment on the porosity, chemical compositon and cellulose crystalline structure of wood cell walls. Carbohyde Polym 155. https://doi.org/10.1016/j.carbpol.2016.08.013
49. Zollfrank C, Fromm J (2009) Ultrastructural development of the softwood cell wall during pyrolysis. Holzforschung 63: 248-253. https://doi.org/10.1515/HF.2009.031

Figures

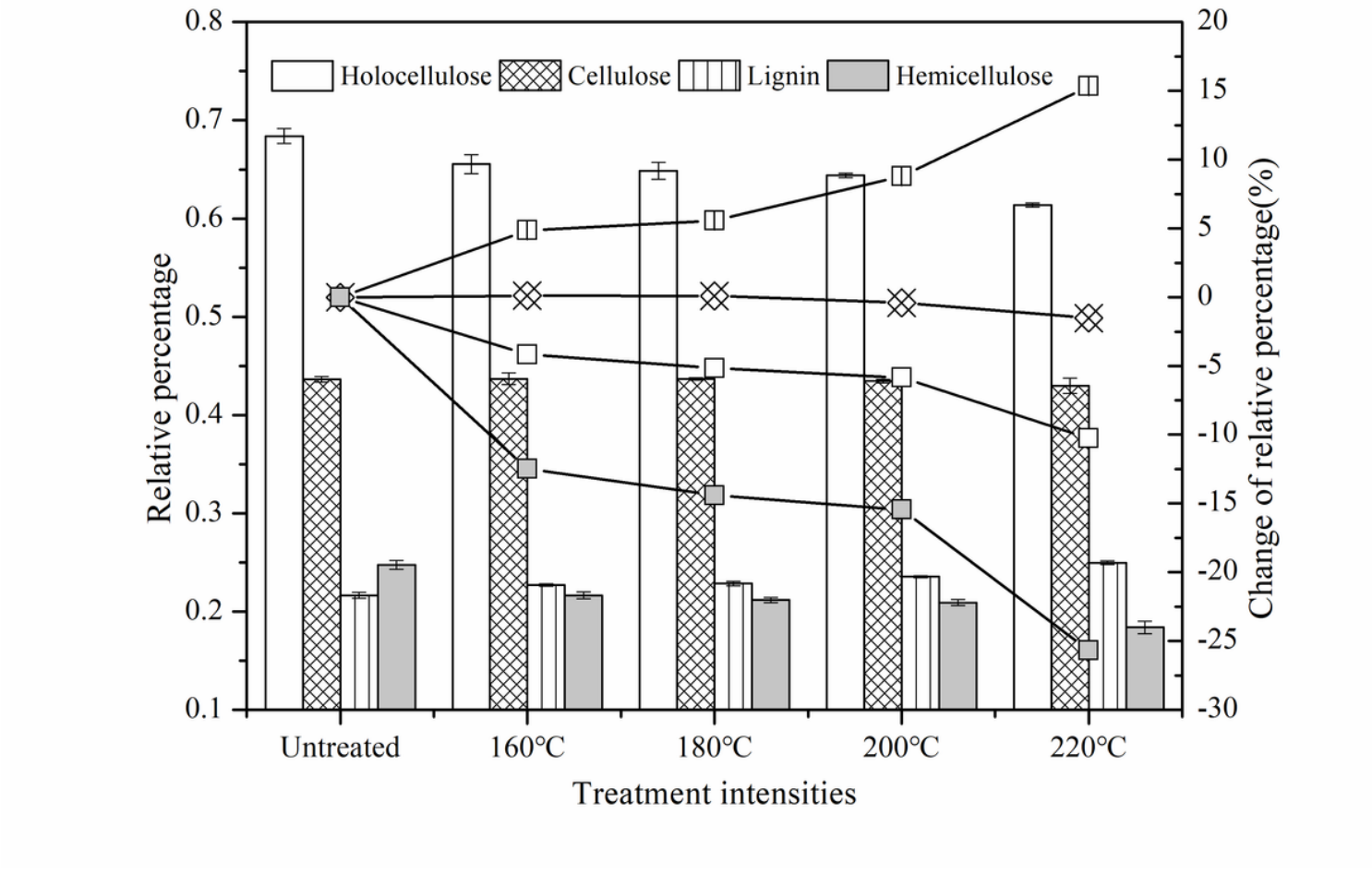

Figure 1

The relative percentages of chemical components of thermally-treated wood as a function of temperature

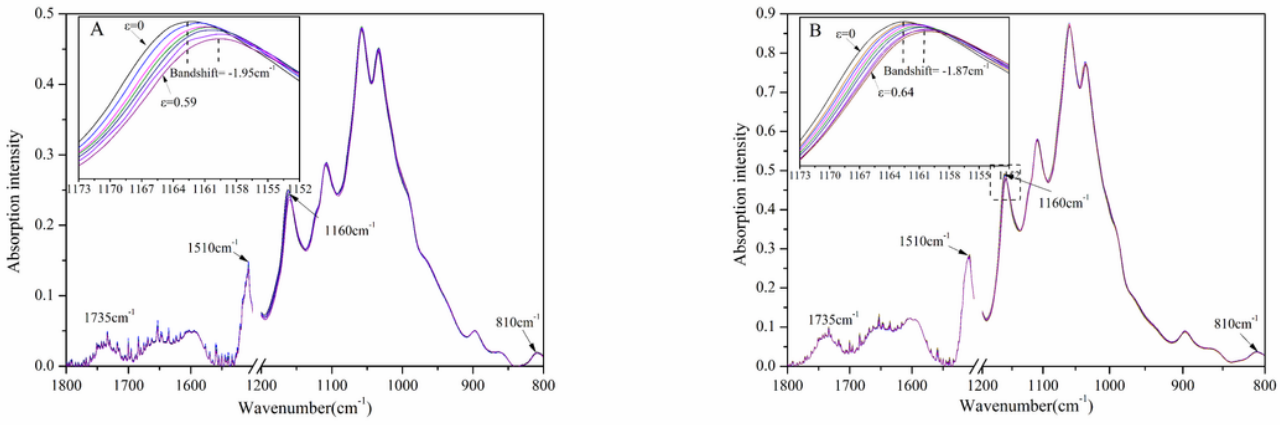

Figure 2

Static FTIR spectra of thermally-treated treatment (A: 180 °C) or untreated (B) wood samples subjected to different strains

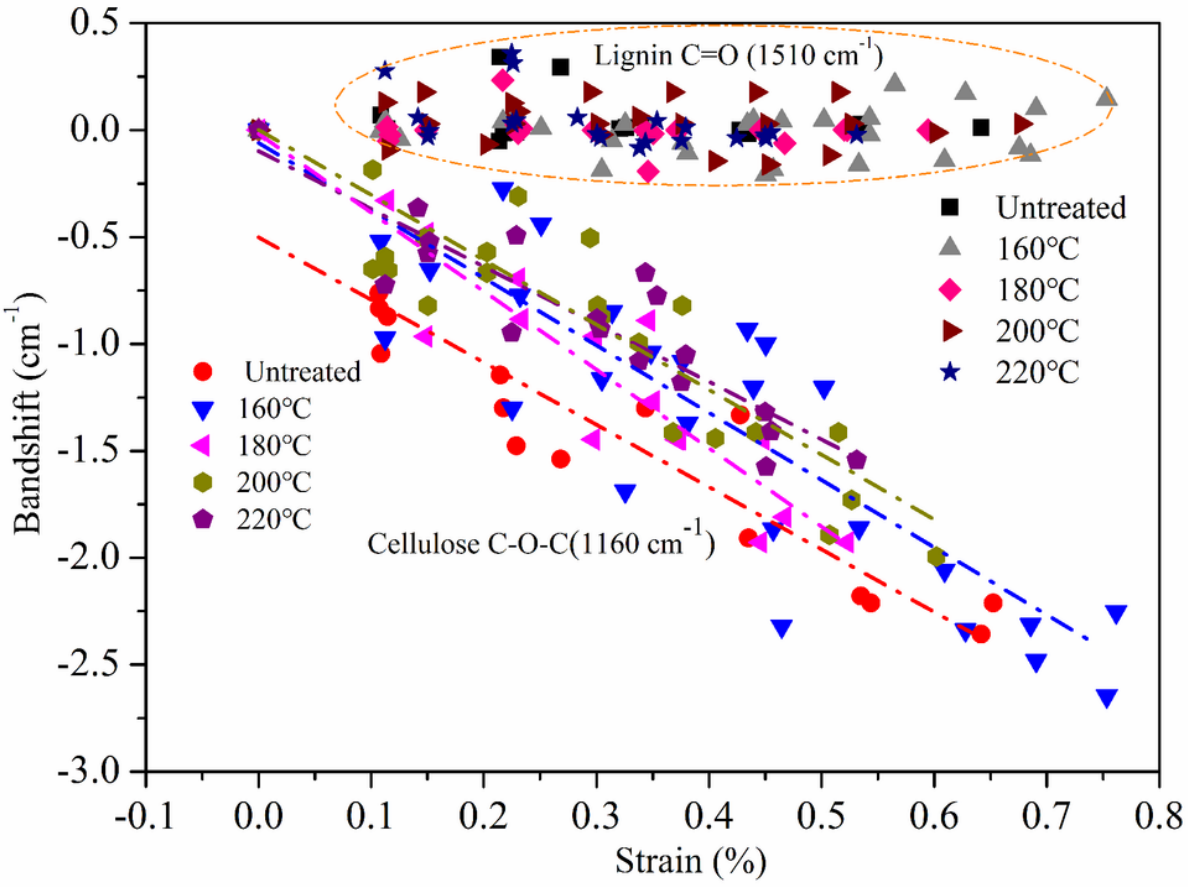

Figure 3

Shifts in the absorption peaks at 1160 cm-1 (cellulose) and 1150 cm-1 (lignin), as a function of the longitudinal strain for samples subjected to different thermal treatments

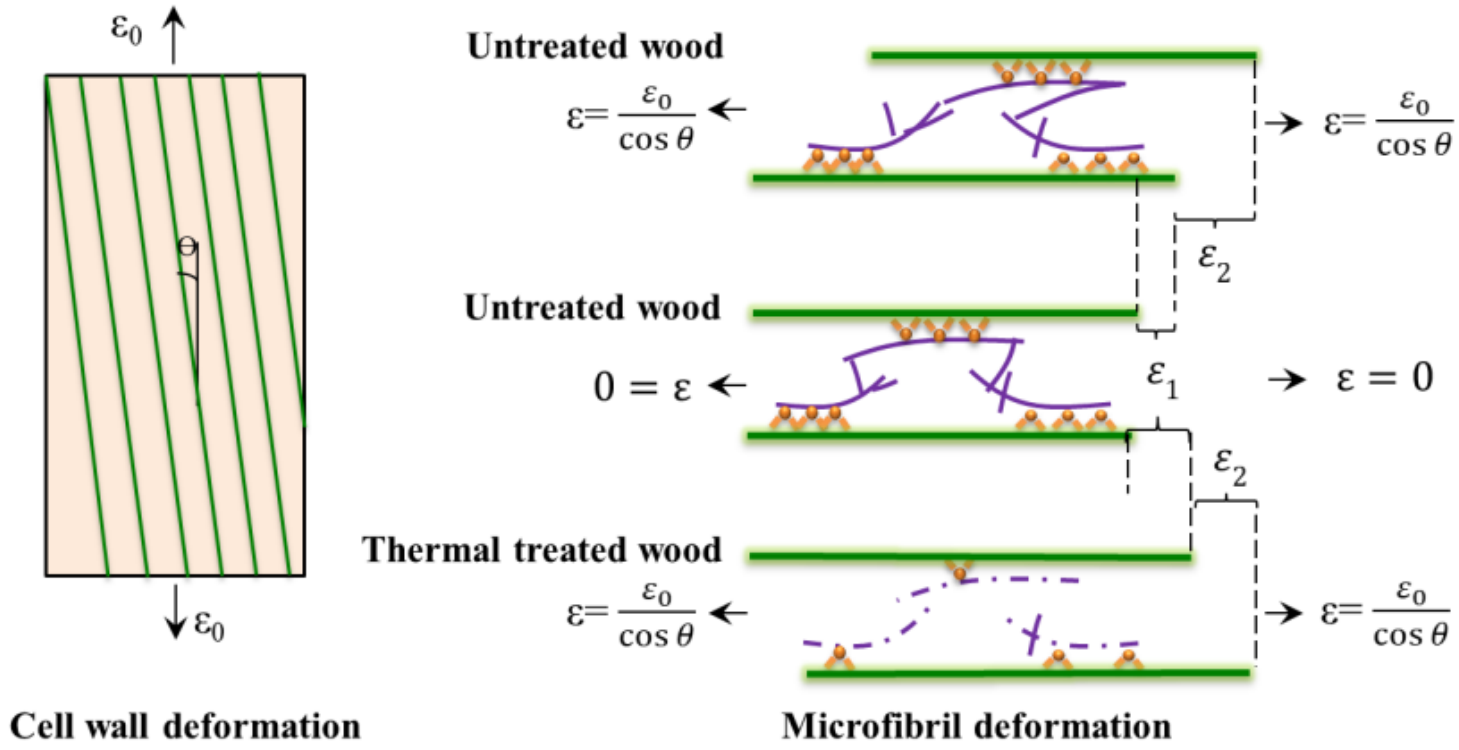

Figure 4

Schematic of cellulose microfibril deformation of untreated and thermally-treated woods, and a depiction of the mesoscale model used here, which represents cellulose microfibrils (green line) interconnected by hemicelluloses (purple curve), and intermolecular hydrogen bonds (orange triangles)

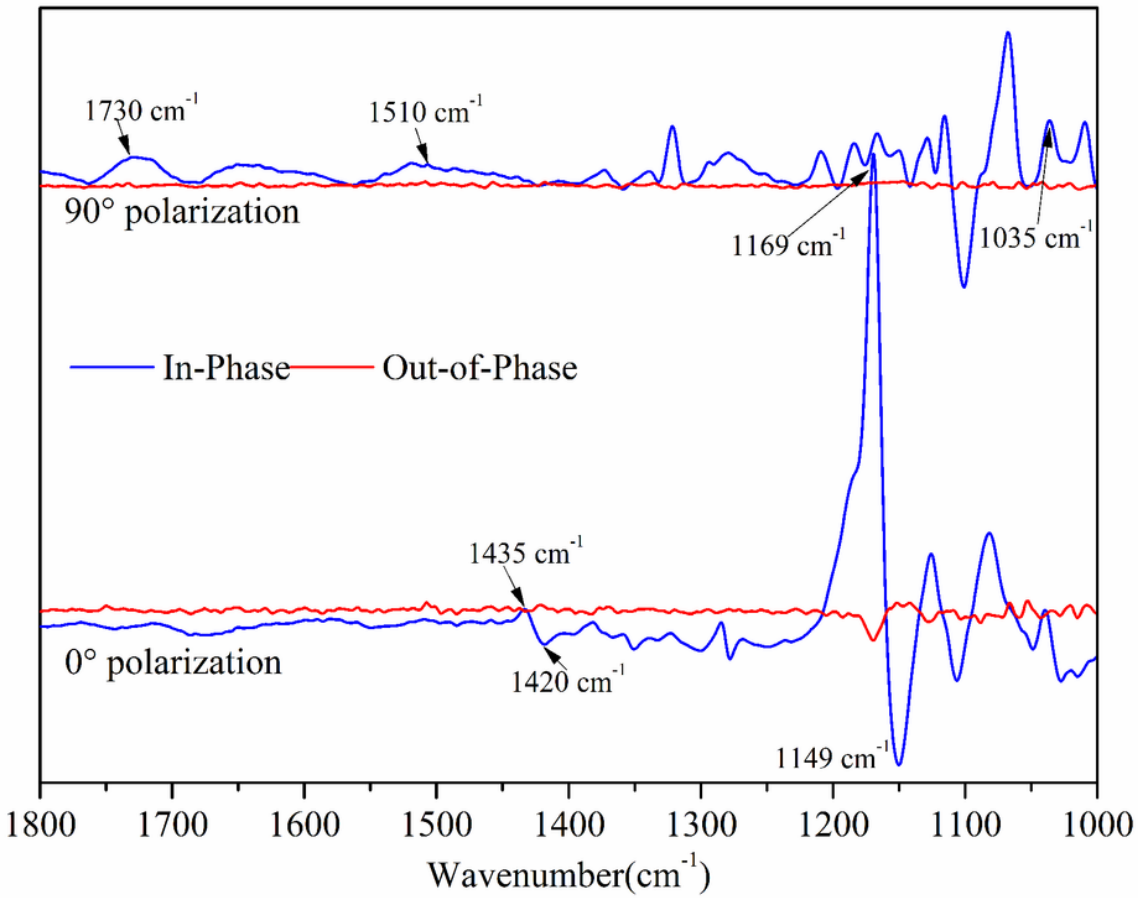

Figure 5

Dynamic mean spectra of the untreated wood sample at 0° and 90° polarization

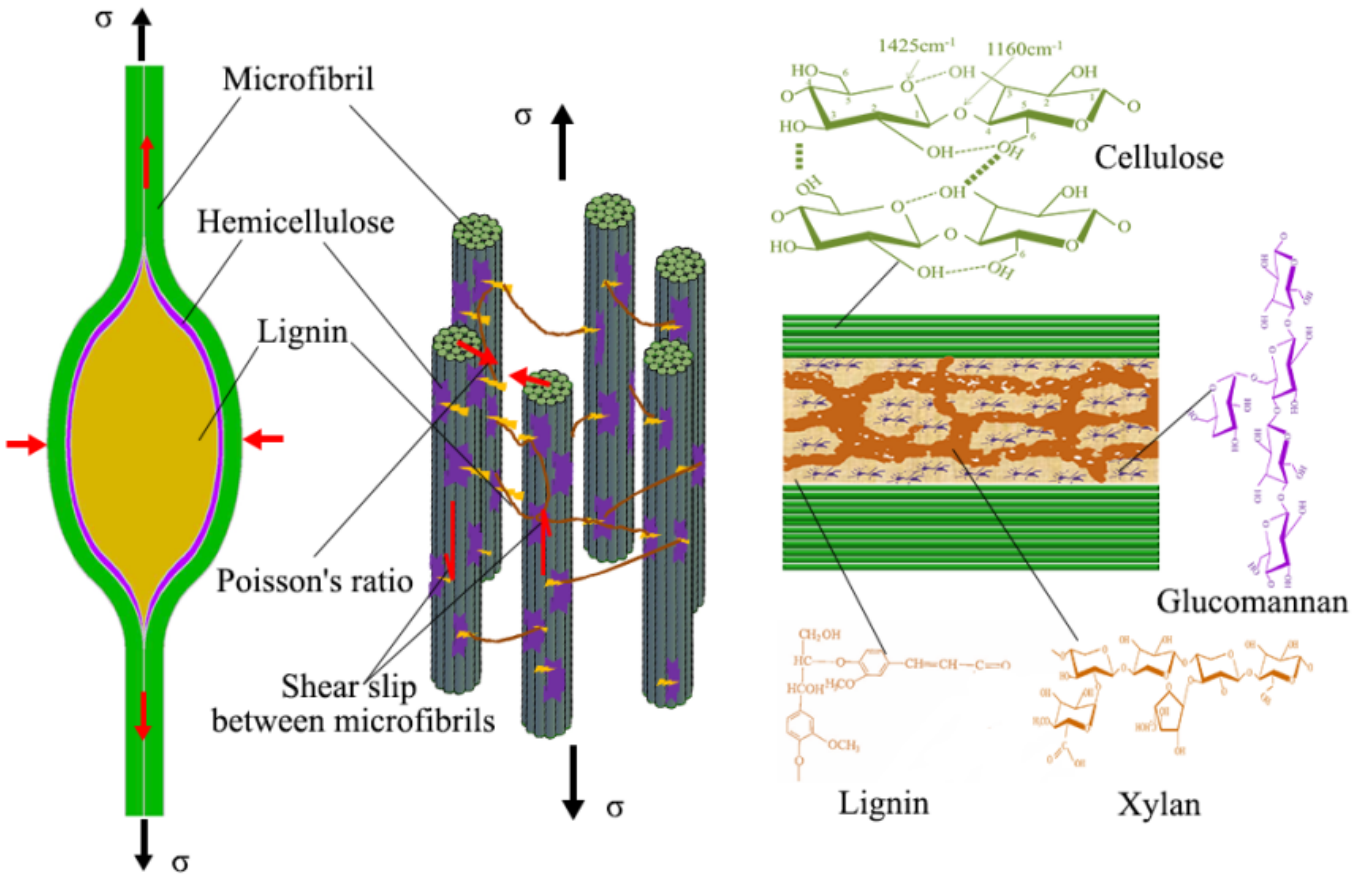

Figure 6

Schematic structure of the cell wall indicating the main structure and alignment of cellulose, hemicellulose, and lignin: modified following an original drawing by Salmén et al. (2016)

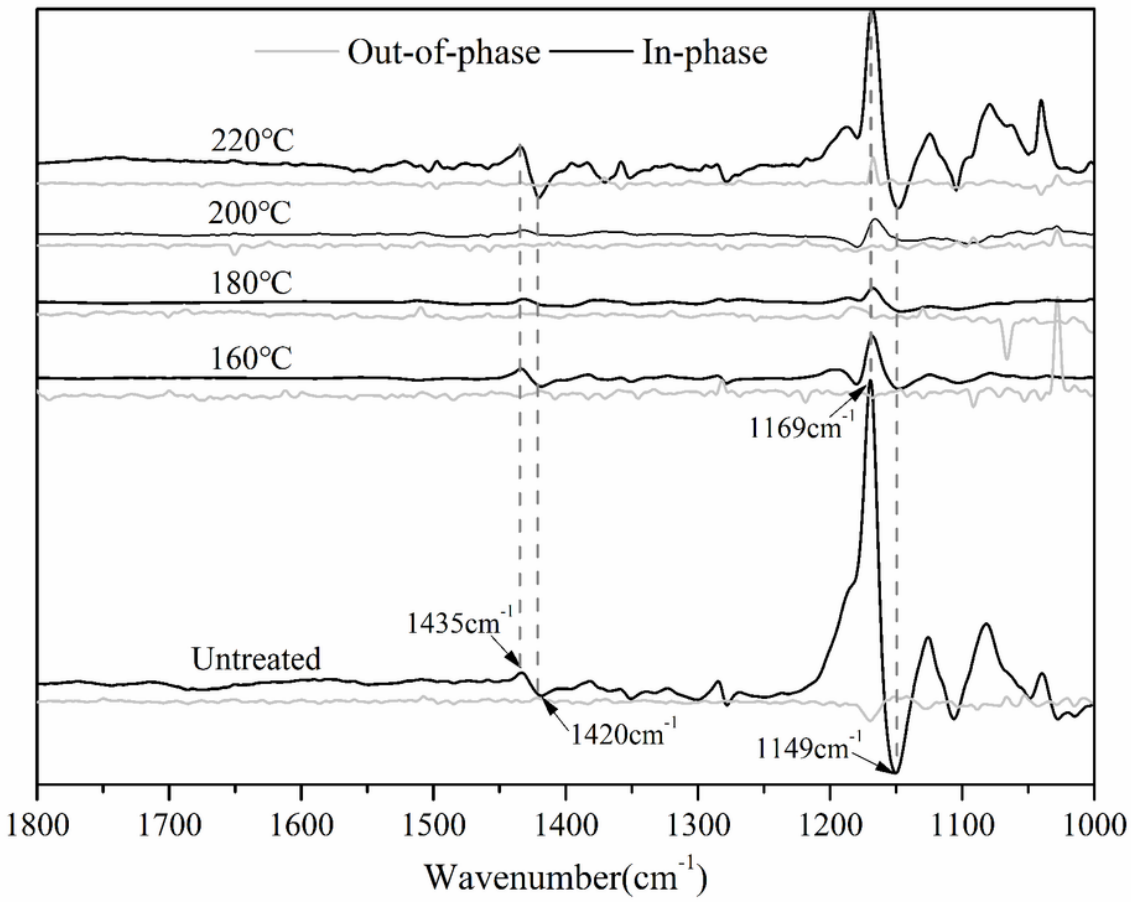

Figure 7

Mean dynamic spectra of the different heat-treated samples measured at 0° polarization

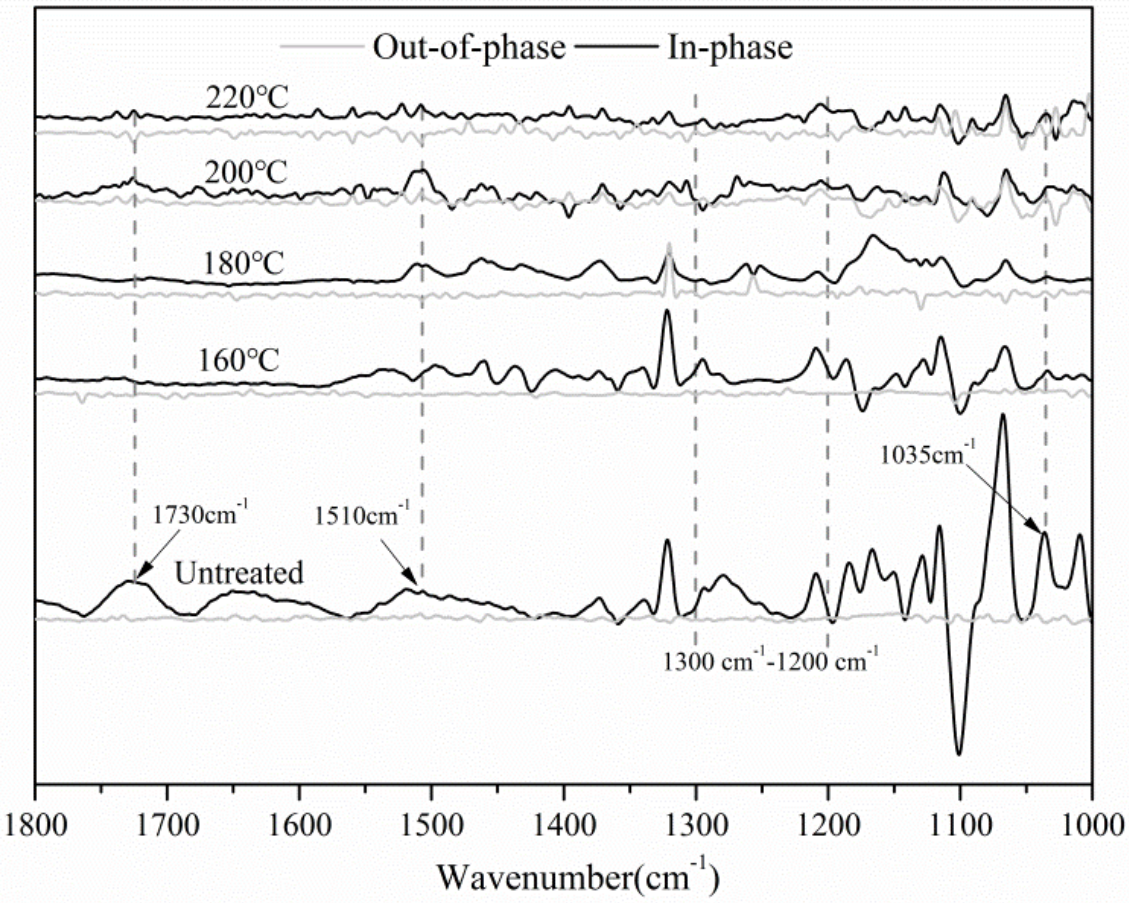

Figure 8

Mean dynamic spectra of samples subjected to different thermal treatments measured at 90° polarization

Supplementary Files

This is a list of supplementary files associated with this preprint. Click to download.

- supplementarymaterials.docx